We are Nitinol.™

Oxidation of Nitinol and Its Effect on Corrosion Resistance

Zhu, Trepanier, Fino, Pelton

ASM Materials & Processes for Medical Device Conference 2003

2003

www.nitinol.com

47533 Westinghouse Drive Fremont, California 94539 t 510.683.2000 f 510.683.2001

Oxidation of Nitinol and its Effect on Corrosion Resistance

L. Zhu, C. Trépanier, A. R. Pelton
Nitinol Devices and Components, Fremont, California, USA

J. Fino
California Polytechnic State University, San Luis Obispo, California, USA

Abstract

This study explores the phase transformations of oxide formation in NiTi and its effects on corrosion resistance. Electropolished Ni-50.8 at% Ti wires were heat treated between 400 and 1000°C for 3 to 300 minutes in air. Surface analytical techniques were used to characterize the thickness, composition and phase distribution of the oxide surface layers. The results of this study suggests that oxidation occurs as follows:

$$NiTi + O_2 \rightarrow Ni_3Ti + TiO_2 \rightarrow Ni_4Ti + TiO_2 \rightarrow Ni + TiO_2$$

The presence, amount, and distribution of these phases depend on both time and temperature. Corrosion behavior of these oxidized wires with respect to the breakdown potential (E_{bd}) by potentiodynamic polarization tests was investigated. The E_{bd} dramatically decreases from 1000mV to below -100mV vs SCE as the oxide thickness increases from less than 0.01µm to 10µm. Above 10µm, however, the oxide forms a protective barrier and the E_{bd} increases to 1000mV. Samples deformed up to 3% strain in bending developed cracks in the protective TiO_2 layer and exposed the Ni-rich phases with a concomitant decrease in E_{bd} to below -100mV vs SCE. These results will be discussed in terms of processing parameters for medical devices.

Introduction

Nitinol is rapidly becoming the material of choice for several implant devices, such as self-expanding stents, due to its superelastic properties. Although several studies have demonstrated good corrosion resistance and biocompatibility which Nitinol provides [1-3], recent studies have shown that in some cases Nitinol implants can corrode *in vivo* and release high nickel content [4, 5]. It has been shown that Nitinol corrosion resistance can be significantly improved by surface treatments such as electropolishing [1]. Electropolishing of Nitinol forms a protective uniform titanium oxide layer that protects the base material from corrosion.

At elevated temperatures in air, titanium reacts with oxygen to form a TiO_2 layer, and the structure of this oxide is important in understanding the biocompatibility of the material. Since several Nitinol implants undergo several heat treatments to shape-set the devices or adjust its transformation temperatures as the final surface treatments, it's also important to assess the effect of oxidation of Nitinol on its corrosion resistance. Several authors [6-12] have studied the effects of surface treatments on the surface composition of NiTi, but the mechanisms of high temperature oxidation and the effects on corrosion are not entirely understood.

Therefore, the goal of this study was to better understand the oxidation of nitinol and determine the effect this oxidation has on corrosion resistance. Furthermore, since most implants are used under stress/strain conditions, the influence of strain on the corrosion resistance of oxidized Nitinol was also assessed.

Experimental Methods and Techniques

Oxidation: Three mm diameter Ni-50.8 at% Ti wire was annealed at 1000°C for 30 minutes, centerless ground to remove the resultant oxide scale, and electropolished. The wire was subsequently oxidized in an air furnace at 400 to 1000°C in 100°C increments for 3, 10, 30, 100, and 300 minutes. Auger Electron Spectroscopy (AES), Focused Ion Beam (FIB), JEOL JSM-5600 Scanning Electron Microscope (SEM), and Oxford Instruments Model 6587 Energy Dispersive X-Ray Spectroscopy (EDXS) were used to characterize the thickness and composition of the oxide layer(s). AES was used for oxide layers up to 0.1µm; FIB between 0.1-1 µm; and SEM was used for ≥ 1 µm layers. Cross-sections of the wires were prepared using standard metallographic techniques. Two sections of wire from each heat treatment condition were mounted in bakelite, polished to a mirror-like finish up to 1200 grit SiC paper, and cleaned in ultrasonicated denatured alcohol. Samples were not etched in order to ensure that all phases were retained for analysis.

Specimens were observed by SEM in both secondary electron imaging (SEI) and backscattered electron imaging (BEI) modes; the BEI mode was especially useful to differentiate Ni-rich (light) and Ti-rich (dark) phases. Layer thickness measurements from AES were based on estimates from the FWHM depth profiles, whereas thicknesses from FIB and SEM were based on averages of measurements from several samples.

Corrosion Testing: In accordance with ASTM F2129, an EG&G Princeton Applied Research potentiostat model 273A was used to conduct the potentiodynamic polarization corrosion tests [13]. The potentiostat is controlled by a computer with 352 SoftCorrIII-DC corrosion test software. A saturated calomel electrode (SCE) is used as a reference electrode for the potential. Two platinum auxiliary electrodes are used as counter electrodes. Testing was conducted in an appropriate polarization cell as recommended in ASTM F2129. The solution was first de-aerated for 30 minutes prior to immersion of the test sample and throughout the test. Then, the Open Circuit Potential (OCP) was monitored for 1 hour. The polarization of the test specimen was then started 100 mV below the OCP at a voltage scan rate of 0.167 mV/sec. The tests were conducted in Hank's simulated physiological solution at an initial pH of 7.4±0.1. The solution was maintained at 37± 1°C using a water bath. The corrosion resistance of the devices was characterized in terms of their breakdown potential (E_{bd}). After testing, the samples were inspected with SEM in both SEI and BEI modes.

Results and Discussion

Oxidation Growth and Composition: No visible oxide was observed by SEM for samples at lower temperatures (≤600˚C) and shorter times (≤30 minutes) at 700°C. These samples were analyzed with AES and/or FIB to determine the oxide thickness and composition. Figure 1 shows the AES depth profile of the electropolished and 400˚C/3 min samples, with a TiO_2 thickness of 110 Å and 200 Å, respectively. After 30 minutes at 400°C, AES revealed a nickel-rich region beneath the outer TiO_2 layer (Figure 2). The remaining samples analyzed with AES showed a more pronounced nickel-rich region below the surface TiO_2 layer.

FIB [14] was used to analyze intermediate oxide thicknesses, as well as to overlap other analysis techniques. Figure 3 shows two light gray superficial platinum layers (marked) that are used as a protective coating during sample preparation. Beneath those layers, a darker TiO_2 (or other Ti suboxide layers) with a lighter nickel-rich sublayer is detected. Chuprina [6] also discovered a "white layer" beneath the surface scale by optical metallography, which he determined to be Ni_3Ti. Voids in the surface layers are also seen in Figure 3. The formation of voids and/or pores may be due to stress generation in the oxide during growth or by the Kirkendall effect whereby vacancies are created when the Ti atoms diffuse away from the NiTi matrix to react with O_2 [6,15-17]. Chu *et al.* [16] suggest that the formation of large voids may be due to the difference in the vertical and lateral oxide growth rates, as well as the collection of vacancies.

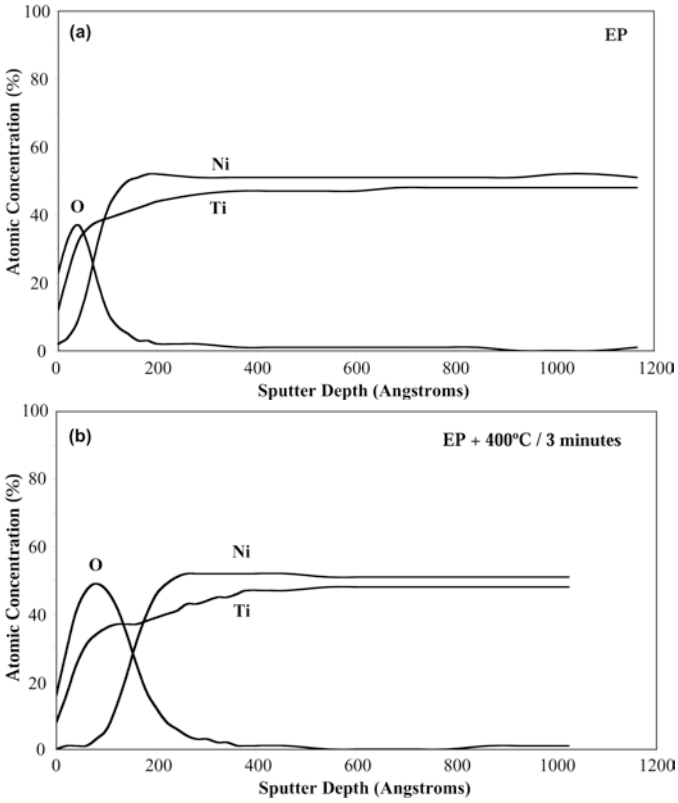

Figure 1: AES depth profiles of NiTi wire: (a) as electropolished; (b) 400°C for 3 minutes

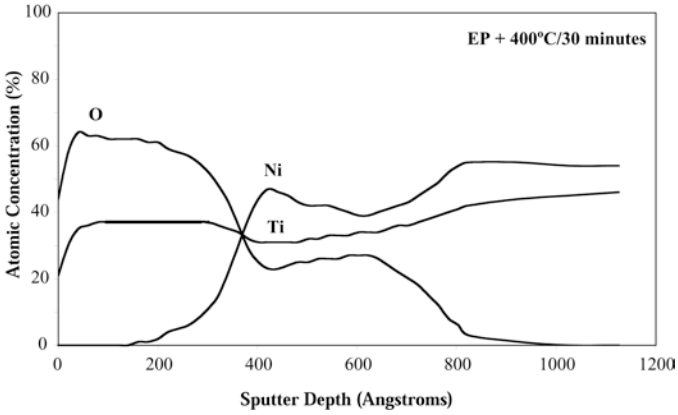

Figure 2: AES depth profile of 400˚C/30 minute NiTi wire. Note the presence of a Ni-rich region below the TiO_2 surface layer

Figure 4 shows the cross-section of the as-electropolished wire, as compared to Figure 5 which illustrates the progressive growth of the oxide with increasing time at 900˚C. The bright interfacial region between the base NiTi and the surface TiO_2 observed for the oxidized samples was analyzed by EDXS to be 75at% Ni and 25at% Ti, consistent with Ni_3Ti (white sublayer); EDXS also confirms the presence of TiO_2 (dark gray). Small Ni_3Ti finger-like projections emerge from the nickel-rich layer and appear to form islands in the oxide. A comprehensive EDXS analysis indicates that the Ni content of the phases increases with increasing distance from the NiTi interface. The Ni_3Ti interfacial layer transforms to Ni_4Ti (80at% Ni), whereas the islands become nearly pure Ni (approximately 92 at% Ni). This composition transition indicates that with increasing time at temperature, the Ni_3Ti sublayer becomes Ti-depleted as the Ti reacts with the O_2, leaving behind nearly pure Ni. The light gray areas embedded in the TiO_2 observed in Figure 5e may be NiO and TiO_2, which can react to form the double-oxide $NiTiO_3$ [18]. Other authors [6-8,15-16] obtained similar results, but there are discrepancies in the actual composition of these phases. X-ray diffraction analysis in Chuprina *et al.* showed the co-existence of Ni_3Ti, Ni, NiO, Ni(Ti), and TiO_2 at high temperatures (>600˚C) [6]. Metallic Ni, oxidized Ni, or Ti atoms in solid solution with Ni (Ni(Ti)) have also been reported [8, 15-16].

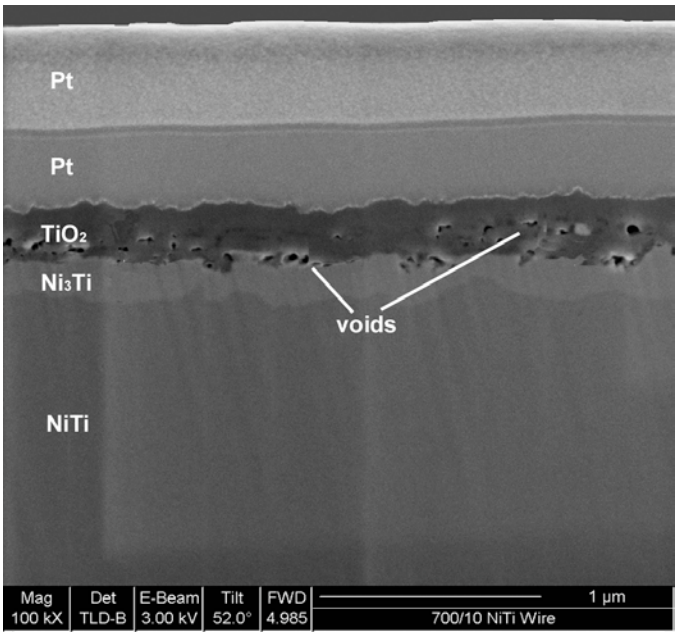

Figure 3: FIB image of 700°C/10 minute NiTi at 100,000X. Note the bright Ni_3Ti layer and (dark) voids

After 3 minutes at 1000°C, the nickel-rich and titanium oxide regions can be easily observed by BEI (see Figure 6a). The nickel-rich precipitates and TiO_2 form a lamellar structure of alternating Ni-rich phases and TiO_2. After 30 minutes at 1000°C, this structure becomes more apparent (see Figure 6b), and after 300 minutes at 1000°C, the oxide has become extremely thick (approximately 300 μm), with most of the Ni from Ni_3Ti dispersing into the TiO_2 layer (see Figure 6c). As Ni diffuses to the surface, it becomes increasingly pure (approximately 98at% Ni), with most of the Ti reacting with O_2 to form TiO_2.

It appears that the TiO_2 layer acts as a diffusion barrier to prevent Ni from oxidizing as expected from pure metal thermodynamics [19]. This is also consistent with the thermodynamic calculations from Firstov *et al*. [15], which indicate that reactions at the NiTi/air interface consist of $NiTiO_3$, TiO_2, and metallic Ni, whereas NiO would not be formed due to insufficient oxygen partial pressures.

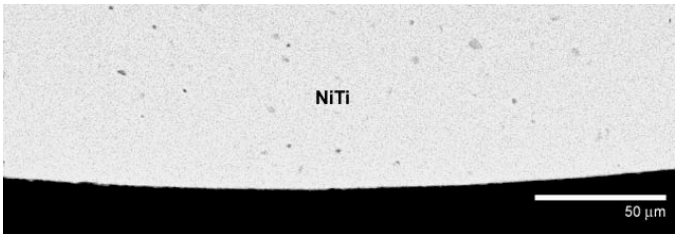

Figure 4:BEI image of as-electropolished cross-section (500X)

Corrosion: The corrosion resistance of the oxidized Nitinol specimens, based on their breakdown potential, depends on the time and temperature of the heat treatment. As shown in Figure 7, while some specimens did not show any localized corrosion, such as the electropolished sample, other specimens showed breakdown potentials as low as -140 mV vs SCE (specimens heat treated at 500 C for 30 min.). The graph in Figure 8 illustrates the variation of the breakdown potential as a function of the oxide layer thickness.

As can be observed from Figure 8, there is a correlation between the breakdown potential and the oxide layer thickness. For oxide layer thickness between 0.01 and 0.05μm, the breakdown potentials remain very high. Then, there is a sharp decrease in the breakdown potential starting from 0.1μm to 10μm thick oxide layer. An increase in the breakdown potential can be observed for specimens with an oxide layer thicker than 10μm. It is important to note that with such a thick oxide layer, the material was insulated from the test solution.

Deformation of the specimen (3% strain in bending) resulted in severe cracking of the oxide layer for specimens with a very thick oxide, which also greatly influenced the corrosion test results. For example, the breakdown potential of the Nitinol specimens heat treated at 400 C for 10 min. decreased from 1030 mV vs SCE to 417 mV vs SCE (Figure 9). In general, a significant decrease in the breakdown potential was observed for the majority of the specimens (Figure 10).

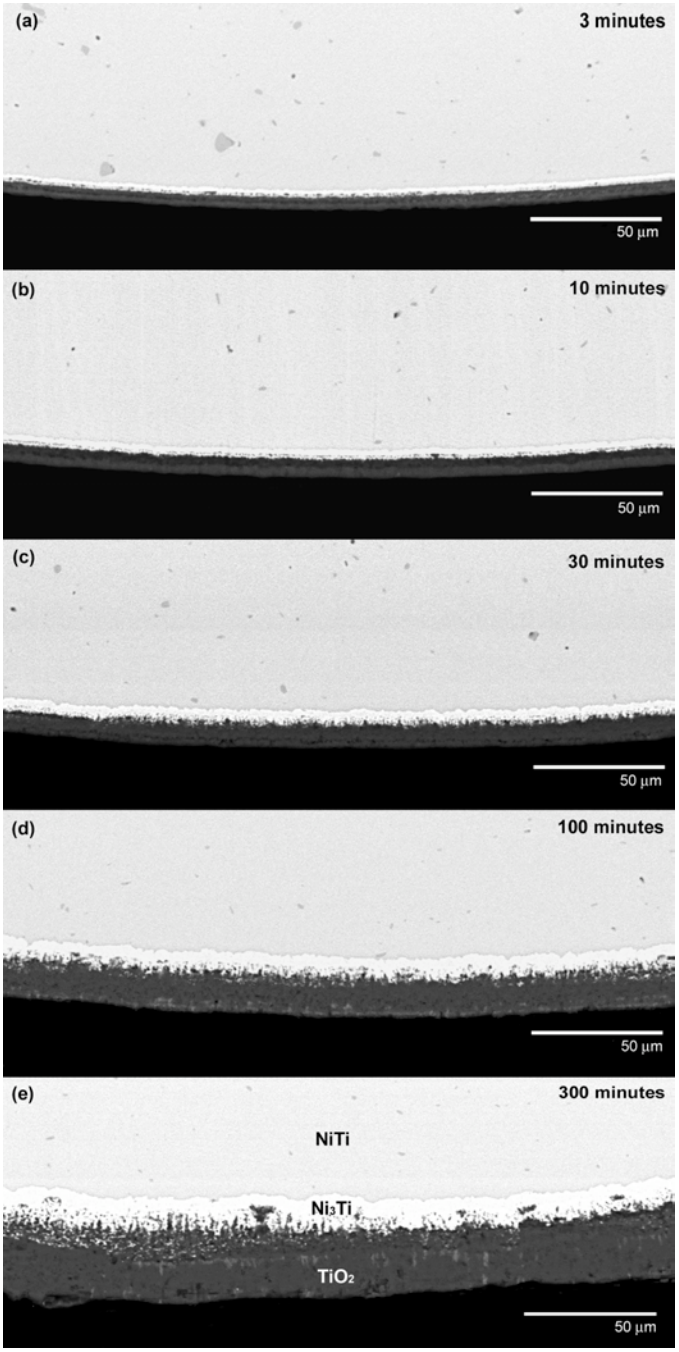

Figure 5: BEI images of NiTi wire cross-section after 900°C: (a) 3 minutes (b) 10 minutes (c)30 minutes (d) 100 minutes (e) 300 minutes. (500X)

As shown, varying mixtures of Ni-riches phases were formed, where the presence, amount, and distribution of these phases depend on time and temperature. Since nickel and nickel compounds have poor corrosion resistance, the presence of nickel-rich phases in the oxide layer of Nitinol can be detrimental to the corrosion resistance of the material if they are exposed to the environment. It is likely that the significant decrease in the corrosion resistance of the specimens with an oxide layer thicker than 0.1µm is due to defects or breaks in the protective TiO_2 oxide layer. Deformation of the specimens up to 3% strain had a similar effect. These observations are in accordance with the results from our visual inspection of the wires after corrosion testing. SEM and EDXS analyses clearly showed that localized corrosion (pitting) initiated in the Ni-rich phase as seen in Figure 11, where the nickel-rich phase appears light gray while the titanium oxide layer appears darker gray.

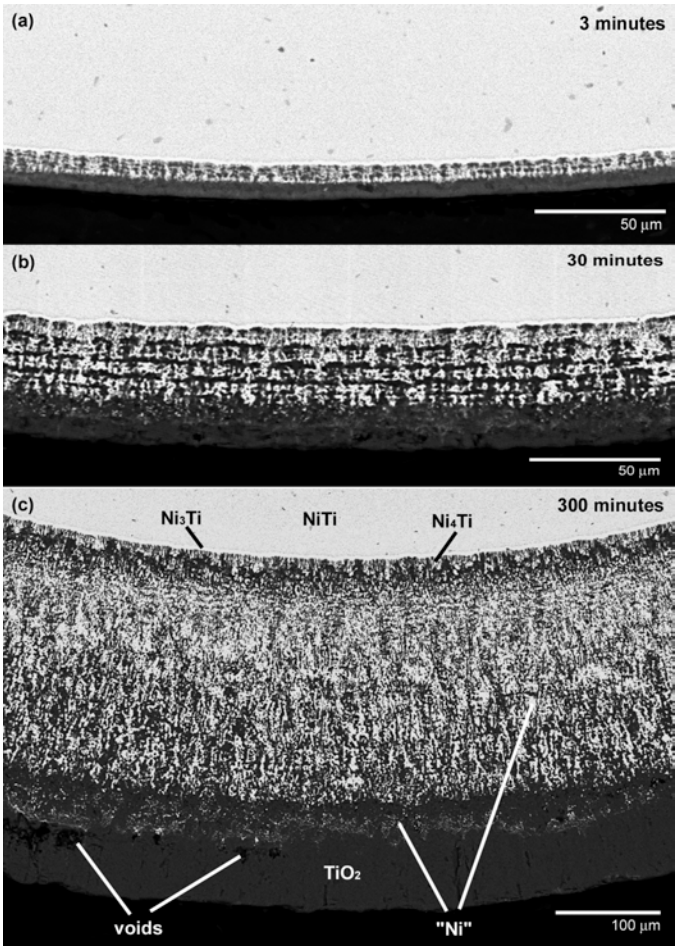

Figure 6: BEI image of NiTi wire cross-section after electropolishing and a heat-treatment at 1000°C: (a) 3 minutes (500X), (b) 30 minutes (500X), (c) 300 minutes (200X)

These results are consistent with the results from a previous study conducted on oxidized Nitinol, which showed that the uniformity and composition of the oxide layer are the determinant factors in the corrosion resistance of Nitinol [1]. Furthermore, because of its superelastic properties, it is likely that Nitinol implants will undergo significant deformation during their use. For example, the physiological strain range for implanted Nitinol stents is about 1-2% strain [20]. It is also not unusual for self-expandable Nitinol stents to be deformed up to 8% strain when constrained in the delivery system before their deployment. As was shown in the present

study, when oxidized Nitinol is deformed, the oxide layer may crack and expose the nickel-rich phases which can significantly lower the corrosion resistance of the material. Since the oxide layer on Nitinol is not superelastic, a thin oxide layer is preferable since it can flex and sustain the large deformations of the underlying Nitinol material without cracking.

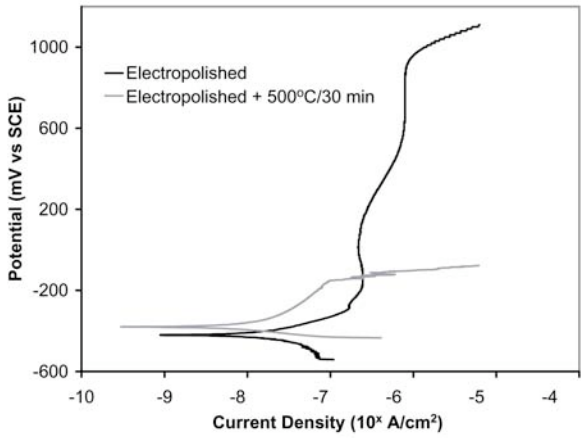

Figure 7: Polarization curves for electropolished and heat treated (500 C for 30 min) specimens.

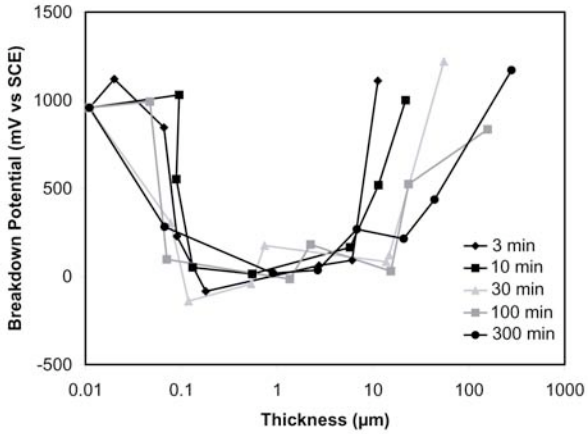

Figure 8: Breakdown potential as a function of oxide layer thickness

Based on these results, if Nitinol implants go through several heat treatments to shape-set or adjust the transformation temperatures of the devices, it is preferable that the implants undergo a final surface treatment to remove the thick oxide layer and passivate the surface. Furthermore, it is important to point out that as opposed to thermally grown oxide that promote the growth of mixed titanium oxide and nickel-rich phases, chemically and electrochemically grown oxide promotes pure titanium oxide formation. During chemical polishing and electropolishing, process nickel is preferentially removed.

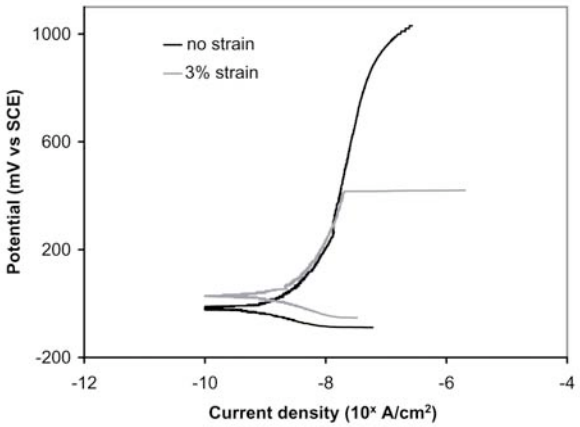

Figure 9: Effect of strain on Nitinol heat treated at 400 C for 10 min.

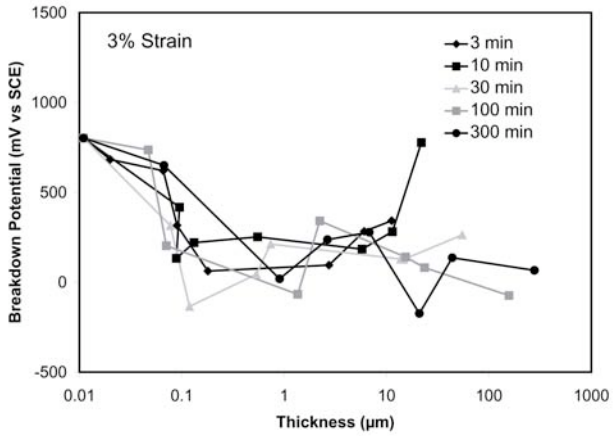

Figure 10: Breakdown potential as a function of oxide layer thickness after 3% strain

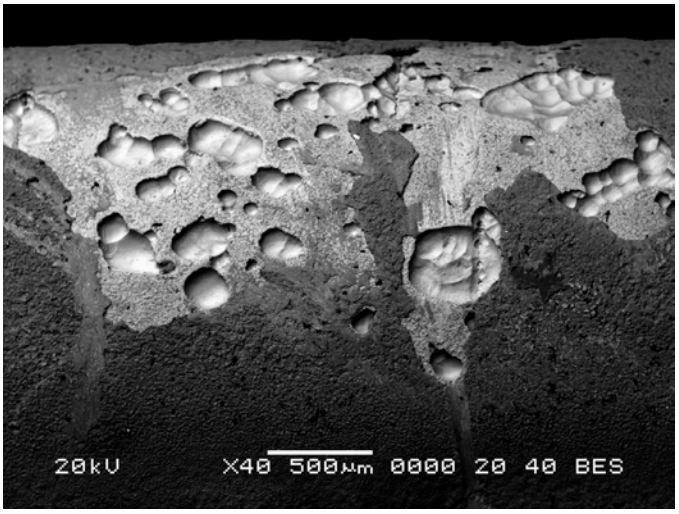

Figure 11: BEI image of pit initiation site on 1000°C, 300 min specimen (3% strain)

Conclusions

The present paper shows the phase transformation for oxidized NiTi. Electropolished wires are characterized by a thin (~0.01µm) TiO_2 layer. The thickness of the oxide layer increases with increasing oxidation time at temperature between 400˚C and 1000˚C. A Ni-rich layer is observed at the interface between NiTi and the thermal TiO_2. Above 800˚C the Ni_3Ti interfacial layer transforms into Ni_4Ti with finger-like projections (approximately 80at% Ni) and Ni islands (approximately 98at% Ni) surrounded by TiO_2. The oxidation reactions for these samples appear to proceed as follows:

$$NiTi + O_2 \rightarrow Ni_3Ti + TiO_2 \rightarrow Ni_4Ti + TiO_2 \rightarrow Ni + TiO_2$$

The breakdown potential dramatically decreases from 1000mV to below -100mV vs SCE as the oxide thickness increases from less than 0.01µm to 10µm. It is likely that the significant decrease in the corrosion resistance of the specimens with an oxide layer thicker than 0.1µm is due to defects or breaks in the protective TiO_2 oxide layer. These superficial cracks expose Ni-rich phases that grow during the oxidation of Nitinol. Above 10µm, however, the oxide forms a protective insulating barrier and the breakdown potential increases to 1000mV. Samples deformed up to 3% strain in bending developed cracks in the protective TiO_2 layer and exposed the Ni-rich phases with a concomitant decrease in breakdown potential to below -100mV vs SCE.

References

1. C. Trépanier, M. Tabrizian, L'H. Yahia, L. Bilodeau, D.L. Piron, in *J Biomed Mat Res (Appl Biomater)* 43, 1998, p. 433.
2. R. Venugopalan, C. Trépanier, in *Min Invas ther & Allied Technol*, 9(2), 2000, p. 67.
3. J. Ryhänen, in *Min Invas ther & Allied Technol*, 9(2), (2000), p. 99.
4. G Riepe, C. Heintz, E. Kaiser, N. Chakfé, M.Morlock, M. Delling, H. Imig, in *Eur J Vasc Endovasc Surg*, 24, 2002, p. 117.\
5. Gimenez-Arnau, A, Riambau, V, Serra-Baldrich, E, Camarasa, JG, in *Contact Dermatitis*, 2000, 43(1), p. 35.
6. V.G. Chuprina, in *Soviet Powder Metallurgy and Metal Ceramics,* 28(4), 1989, p. 468-472.
7. J.P. Espinos, A. Fernandez, and A.R. Gonzalez-Elipe, in *Surf Sci,* 295, 1993, p. 402-410.
8. R.G. Vichev, *et al.*, in Proceeding of the Seventh European Conference on Applications of Surface and Interface Analysis, eds. I. Olefjord, L. Nyborg, and D. Briggs (Goteborg), 1997, p. 679-682.
9. C. Trepanier, *et al.*, in *J Biomed Mater Res (Appl Biomater)*, 43, 1998, p. 433-440.
10. S. Trigwell, *et al.*, in *Sufr Interface Anal*, 26, 1998, p. 483-489.
11. L. Zhu, J. Fino, A.R. Pelton, in SMST-2003: Proceedings of the International Conference on Shape Memory and Superelastic Technologies, 2003, in press.
12. C. Trepanier et al, in SMST-2003: Proceedings from the International Conference on Shape Memory and Superelastic Technologies, 2003, in press.
13. F2129-01, Annual Books of ASTM Standards, Medical Devices and Services, vol. 13.01, 2001.
14. B.L. Pelton and J. Vitarelli, in SMST-2000: Proceedings from the International Conference on Shape Memory and Superelastic Technologies, eds. S.M Russell and A.R. Pelton, (Pacific Grove, California: International Organization on SMST-2000), p. 97-102.
15. G.S. Firstov, *et al.*, in *Biomaterials,* 22, 2002, p. 4863-4871.
16. C.L. Chu, S.K. Wu, and Y.C. Yen, in *Materials Science and Engineering*, A216, 1996, p. 193-200.
17. A.S. Khanna, High Temperature Oxidation and Corrosion, ASM International, 2002.
18. C.L. Zeng, in *Oxidation of Metals*, 58(1/2), 2002, p. 171-184.
19. D.R. Gaskell, Introduction to Metallurgical Thermodynamics, 2nd ed., 1981, p. 287.
20. T. Lopes, X. Gong, C. Trépanier, in SMST-2003: Proceedings of the International Conference on Shape Memory and Superelastic Technologies, 2003, in press.